Journal of Cluster Science (2019) 30:985–994
https://doi.org/10.1007/s10876-019-01558-z

ORIGINAL PAPER

Sunlight-Mediated Antibacterial Activity Enhancement of Gold Nanoclusters and Graphene Co-decorated Titanium Dioxide Nanocomposites

Tong Zhou[1] · Yan Cheng[2] · Haiyuan Zhang[2] · Guixia Wang[1]

Received: 18 February 2019 / Published online: 19 April 2019

Abstract

Titanium dioxide (TiO_2) as one of the most important biocompatible semiconductor nanomaterials, has been widely used as antibacterial agents. However, since it is only active under ultraviolet radiation, its application has been dramatically limited. Here, TiO_2 nanoparticle (NP)-Au nanocluster (NC)-graphene (TAG) nanocomposites were designed to improve the antibacterial activity of TiO_2 NPs under sunlight condition. Incorporation of Au NCs and graphene into TiO_2 NPs can significantly enhance the solar energy utilization efficiency and promote the electron–hole separation, leading to enhanced reactive oxygen species (ROS) production in TAG, as evidenced by dihydrorhodamine 123 and DCF assays. Bacterial growth inhibition assessments revealed that TAG nanocomposites possessed more potent antibacterial activity against both gram-negative Escherichia coli (*E. coli*) and gram-positive Staphylococcus aureus (*S. aureus*) bacteria than TiO_2 NPs alone. Scanning electron microscope images of bacteria further displayed that TAG could cause severe damage on the surface membrane structure of both *E. coli* and *S. aureus* bacteria. Intracellular ROS production, glutathione depletion, and lipid peroxidation of bacteria were found to be elicited by TAG, suggesting the molecular mechanism underlying their antibacterial activity is possibly based on oxidative stress.

Keywords Graphene · Sunlight radiation · Antibacterial activity · Titanium dioxide · Gold nanoclusters

Introduction

Antibacterial agents are very important in water disinfection, food packaging, medicine and textile industry [1]. Traditional organic compound-based antibacterial agents have been widely applied in these fields, however, their disadvantages of volatility, toxicity, poor heat resistance, easy solution, adverse side effects, and multiple drug resistance have dramatically limited their further application [2]. This prompts the development of alternative strategies for inactivation of bacteria. Nanomaterials with unique physicochemical properties are emerging as new antibacterial agents because they are stable and low-toxic, and able to directly destroy bacteria without targeting a specific step in their metabolic pathway as most organic compound-based antibacterial agents did [3–6].

The semiconductors-based photocatalysis for bacterial inactivation has emerged with inestimable superiority as an alternative green method for water disinfection in recent years [7]. Titanium dioxide (TiO_2) as one of the most important semiconductor nanomaterials, has been widely used as an antibacterial agent in the past few decades due to their photoinduced electrons and holes that facilitate the generation of reactive oxygen species (ROS) to inhibit the bacterial growth [8–10]. Since sunlight is abundant in nature, development of new antibacterial nanomaterials that can efficiently utilize the solar energy is necessary.

Electronic supplementary material The online version of this article (https://doi.org/10.1007/s10876-019-01558-z) contains supplementary material, which is available to authorized users.

✉ Yan Cheng
ycheng@ciac.ac.cn

✉ Guixia Wang
gwang168@jlu.edu.cn

[1] Department of Endocrinology and Metabolism, the First Hospital of Jilin University, Jilin University, Changchun 130061, Jilin, People's Republic of China

[2] Laboratory of Chemical Biology, Changchun Institute of Applied Chemistry, Chinese Academy of Sciences, Changchun 130022, Jilin, People's Republic of China

However, the wide band gap energy (3.0–3.2 eV) [11, 12] of TiO_2 makes them only active under ultraviolet (UV) radiation, which dramatically reduces their solar utilization efficiency because about 96% of photons from solar energy have wavelengths larger than 385 nm at the earth's surface [13]. Moreover, the fast recombination of photoinduced electrons and holes on TiO_2 nanomaterials can significantly reduce the efficiency of ROS generation, ultimately resulting in lowered antibacterial activity. Many efforts have been made to advance the antibacterial activity of TiO_2 nanomaterials through enhancement of their solar utilization efficiency or inhibition of the recombination of electron–hole pairs. For example, sulphur was doped into TiO_2 nanoparticles (NPs) to reduce the band gap energy of TiO_2 NPs and facilitate hydroxyl radical generation under visible light radiation, resulting in significantly enhanced damage to Micrococcus lylae [14], and silver was deposited on the surface of TiO_2 NPs to trap the electron excited from TiO_2 NPs, preventing electron excited from TiO_2 NPs, preventing the recombination of electron–hole pairs [15] and showing excellent antibacterial activity against Escherichia coli (E. coli) bacteria.

Au nanoparticles have been reported to enhance the photocatalytic and antibacterial activity of TiO_2 under sunlight radiation, however, the efficiency for utilizing solar light is low because it can only absorb sunlight with the wavelength near 550 nm caused by the localized surface plasmon resonance effect [16–18]. It has been reported that the energy gap between the highest occupied molecular orbital (HOMO) and the lowest unoccupied molecular orbital (LUMO) of gold nanoclusters (Au NCs) is ranging from 1.4 to 1.7 eV [19, 20]. It means Au NCs (A) can be excited by the photons at the wavelength smaller than 729 nm, which makes them as ideal sensitizers under sunlight exposure. For example, $Au_{25}(SR)_{18}$ NCs loading onto TiO_2 give rise to largely enhanced photocatalytic activity under visible light radiation, where $Au_{25}(SR)_{18}$ NCs act as small-band-gap semiconductors to absorb visible light and promote electron–hole separation; [21]; Au NCs loading on $BaLa_4Ti_4O_{15}$ photocatalyst can enhance the water splitting performance [22]; Au NCs also can effectively enhance the rate of hydrogen evolution when they are loaded on TiO_2 because Au NCs have higher LUMO energy (− 0.63 V versus reversible hydrogen electrode (RHE)) [20] than the conduction band (CB) energy (− 0.51 V versus RHE) [23, 24] of TiO_2 NPs, facilitating the electron transfer from LUMO of Au NCs to CB of TiO_2 NPs and the hole staying at HOMO of Au NCs. As a result, incorporation of Au NCs onto TiO_2 NPs can significantly enhance the absorption in the visible region and introduce free electrons and holes under sunlight radiation.

The fast recombination is another problem which reduces the efficiency of ROS generation. Graphene, with mobility exceeding 15,000 $m^2\ V^{-1}\ s^{-1}$ at room temperature [25, 26], could effectively inhibit electron–hole recombination. Graphene–TiO_2 nanocomposites have been previously designed to raise the performance of TiO_2 in photocatalytic and antibacterial activity. For example, graphene-wrapped anatase TiO_2 NPs were reported to possess excellent photocatalytic property due to the hindrance of the recombination of excited electrons [27]; graphene–TiO_2 nanocomposites show much higher antibacterial activity against *E. coli* bacteria than original TiO_2 nanocrystals [28].

In the present study, TiO_2 NP-Au NC-graphene (TAG) nanocomposites were designed to sufficiently utilize solar energy and facilitate the electron–hole separation in purpose of improving the antibacterial activity of TiO_2 NPs. As shown in Fig. 1, under sunlight radiation, the electron of Au NCs can be excited from HOMO to LUMO and transfer to CB of TiO_2 NPs, and ultimately to graphene due to the staggered energy levels, leaving holes in HOMO. Moreover, the electrons in valence band (VB) of TiO_2 can also be excited by the UV portion of sunlight, and the generated electrons and holes can transfer to graphene and Au NCs, respectively. After this efficient electron–hole separation, free electrons in graphene and free holes in Au NCs can react with oxygen (O_2) and water (H_2O) to form superoxide radical anion ($O_2{\cdot}^-$) and hydroxyl radical (·OH), respectively, resulting in more significantly enhanced antibacterial activity of TAG nanocomposites compared to TiO_2 NP-graphene (TG), TiO_2 NP-Au NC (TA) nanocomposites and TiO_2 NPs (T) alone. The antibacterial activity was investigated in both gram-negative *E. coli* and gram-positive Staphylococcus aureus

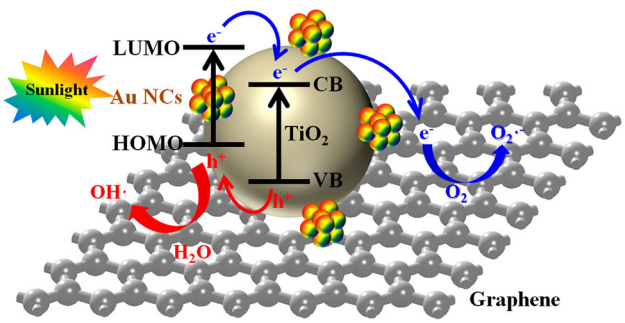

Fig. 1 Schematic illustration of electron transfer and ROS generation mechanism on TAG under sunlight radiation. The narrow band gap of Au NCs facilitates the electrons to be excited from HOMO to LUMO under sunlight radiation, and the staggered energy bands further promote the electrons transferring to CB of TiO_2 NPs, and ultimately to graphene matrix, forming the free electrons and subsequent superoxide radicals. Holes left behind by electrons on HOMO of Au NCs and transferred from VB of TiO_2 NPs can form hydroxyl radicals

(*S. aureus*) bacteria, and the potential mechanism was clarified.

Materials and Methods

Materials

TiO_2 (commercial P25) was purchased from Degussa Co., Ltd., Germany. Graphite, sodium nitrate, potassium permanganate, sulphuric acid (98%), H_2O_2, hydrochloric acid, Glutathione (GSH), chloroauric acid, sodium dodecyl sulfate (SDS), dithiothreitol (DTT), 5,5-dithio-bis-(2-nitrobenzoic acid) (DTNB), thiobarbituric acid (TBA), trichloroacetic acid (TCA), hydrochloric acid (HCl) were purchased from Aladdin (Shanghai, China). Pure water (18.2 MΩ) was obtained from a Milli-Q water purification system (Millipore, Bedford, MA) in all experiments.

Preparation of TG, TA, and TAG

Graphene oxide (GO) and Au NCs were firstly synthesized according to the reported method [29, 30]. For TA preparation, 20 mL of TiO_2 NPs aqueous suspension (10 mg ml^{-1}) was added into 20 mL of as-prepared Au NCs (20 mM) suspensions, and the resulting suspension was allowed to stir for 5 h. After centrifugation, the achieved TA nanocomposites were washed with water and dried at 80 °C for 12 h. For TG and TAG preparation, 100 mg TiO_2 (or TA) was added to GO solution (30 mL of H_2O and 15 mL of anhydrous ethanol) with vigorous stirring for 2 h, resulting in a homogeneous suspension. Then, this suspension was transferred to a 100 mL-Teflon-sealed autoclave and maintained at 120 °C for 3 h. After centrifugation and washing by water, achieved TG and TAG were dried at 80 °C.

Physicochemical Characterization of T, TG, TA, and TAG

The X-ray diffraction (XRD) patterns were recorded on a Rigaku X-ray diffractometer using Cu K*a* radiation operated at 40 kV and 200 mA. The morphology was characterized using a JEM-2010 transmission electron microscope (TEM) at an accelerating voltage of 200 kV. The contents of Au NCs were determined by inductively coupled plasma optical emission spectrometry (ICP-OES, Thermo Scientific iCAP6300). Diffuse reflectance ultraviolet–visible (UV–Vis) spectra was recorded with Perkin Elmer UV–Vis Spectrometer Lambda 35 by using $BaSO_4$ as a reference material. Infrared (IR) spectrum was recorded with VERTEX 70 fourier transform infrared spectrometer. Dynamic light scattering (DLS) measurements were performed on a Malvern Zetasizer Nano ZS apparatus.

Detection of Photoinduced ROS

Total ROS were determined by dihydrorhodamine 123 (DHR123) and 2′,7′-dichlorodihydrofluorescein diacetate (H_2DCFDA), which can react with ROS to exhibit the increased fluorescence [31–33]. For DHR123 assay, to each well of a 96 multiwell black plate we added 80 μL of DHR123 working solution (20 μM) and 20 μL of nanoparticle suspension (1000 μg mL^{-1}), followed by radiation with or without simulated sunlight for 15 min. After 2 h of incubation, the fluorescence emission spectra of DHR123 in the range of 500–600 nm were collected using a SpectraMax M3 microplate reader with an excitation wavelength of 490 nm. Similar procedure was also performed for H_2DCFDA (10 μM) assay, and the fluorescence emission spectra were collected in the range of 500–600 nm with an excitation wavelength of 490 nm.

Antibacterial Assessments

Monocolonies of *E. coli* and *S. aureus* were grown at 37 °C for 12 h under 160 rpm rotation in liquid Luria–Bertani (LB) culture medium (yeast extract 5 g, tryptone 10 g and NaCl 5 g in 1 L of deionized water at pH = 7.3). As for antibacterial experiments, the bacteria concentrations were determined by measuring the optical density at 600 nm (OD_{600}). 50 μL of a stepwise concentration gradient (0, 9.375, 18.75, 37.5, 75, 150, 300, 600, 1200, and 2400 μg mL^{-1}) of T, TG, TA, and TAG suspensions was prepared in LB culture medium and placed in a 96 well cell culture plate. 100 μL of *E. coli* or *S. aureus* bacterial suspension (OD_{600} = 0.1) was then inoculated into each well. The above procedure was performed in duplicate: one plate was radiated with simulated sunlight (Sun 2000 Solar Simulator, Abet Technologies) for 30 min, followed by 6 h of incubation at 37 °C at 160 rpm rotation; the other plate was only incubated at 37 °C for 6 h at 160 rpm rotation without sunlight radiation. The value of OD_{600} was recorded every hour. In addition, colony forming capability was evaluated on agar LB plates. 50 μL of 600 μg mL^{-1} particles in LB was mixed with 100 μL of bacterial suspension (OD_{600} = 0.1), and the resulting suspension was radiated with simulated sunlight for 30 min, followed by 2 h of incubation at 37 °C at 160 rpm rotation, or only incubated at 37 °C for 2 h at 160 rpm rotation without sunlight radiation. Then, the resulting bacterial suspension was diluted for 10,000 times, and 50 μL of the suspension was spread on agar plate. The number of the colonies was counted after 24 h of incubation at 37 °C.

Live/Dead Staining for Assessment of Antibacterial Activity

500 μL of 600 μg mL^{-1} T, TG, TA, or TAG suspensions were prepared in LB culture medium and placed in a 6-well cell culture plate. 1000 μL of *E. coli* or *S. aureus* bacterial suspension (OD_{600} = 0.1) was then added into each well. The above procedure was performed in duplicate: one plate was radiated under simulated sunlight for 30 min, followed by 2 h of incubation at 37 °C at 160 rpm rotation; the other one was only incubated at 37 °C for 2 h at 160 rpm rotation without sunlight radiation. 1 mL of the above solution was centrifuged at 10,000*g* for 10 min, and then the pellets were re-suspended in 1 mL of LB culture medium. The bacterial suspension was stained by SYTO9 (10 μM) and propidium iodide (PI, 10 μM) for 30 min under dark condition at room temperature. Then, the bacterial suspension was centrifuged at 10,000*g* for 10 min and re-suspended in 1 mL of PBS buffer. 5 μL of the stained bacterial suspension was trapped between a slide and a coverslip, and the fluorescence images were taken by Nikon Ti-S fluorescence microscope (Tokyo, Japan) with 40 × objective.

Scanning Electron Microscopy (SEM) Observation of Bacteria Treated with TAG Nanocomposites

50 μL of 600 μg mL^{-1} TAG suspension in LB was mixed with 100 μL of *E. coli* or *S. aureus* bacterial suspension (OD_{600} = 0.1), and the resulting suspension was radiated with simulated sunlight for 30 min, followed by 2 h of incubation at 37 °C at 160 rpm rotation, After centrifugation, the TAG-treated or untreated bacteria were harvested and fixed with 2.5% glutaraldehyde solution in 4 °C overnight. Then, the samples were sequentially dehydrated with 30, 50, 70, 90, and 100% ethanol for 20 min, respectively. Finally, the sample dispersed in 100% ethanol was dropped on silicon wafer and coated with gold in a sputter coater. SEM images were taken by Scanning Electron Microscopy (Hitachi S-4800-II).

Intracellular ROS, Lipid Peroxidation and GSH Assessments

500 μL of 600 μg mL^{-1} T, TG, TA, or TAG suspensions were prepared in LB medium and placed in a 6-well cell culture plate. 1000 μL of *E. coli* or *S. aureus* bacterial suspension (OD_{600} = 0.1) was then added into each well. The above procedure was performed in duplicate: one plate was radiated with simulated sunlight for 30 min, followed by 6 h of incubation at 37 °C at 160 rpm rotation; the other plate was only incubated at 37 °C for 6 h at 160 rpm rotation without sunlight radiation. For intracellular ROS detection, 1 mL of the bacterial suspension was collected by centrifugation and incubated with 1 mL of LB medium containing 10 μM H_2DCFDA for 30 min under dark condition. Then the cells were centrifuged and dispersed in 200 μL of PBS buffer. 5 μL of the stained bacterial suspension was trapped between a slide and a coverslip, and the fluorescence images were taken by Nikon Ti-S fluorescence microscope (Tokyo, Japan) with 40 × objective. For lipid peroxidation experiment, SDBME buffer was used for cell lysis. 1 mL of the above bacterial suspension was collected by centrifugation and incubated with 100 μL of SDBME buffer (4.5 mg Tris–HCl, 2.66 mg Tris-base, 30 μL of 10% SDS, 200 μL of 1 M DTT and 770 μL of H_2O) for 15 min of lysis in boiling water bath. Then, 100 μL of TBA-TCA-HCl reagent (2 μL of concentrated HCl, 98 μL of H_2O, 14.72 mg TCA, and 0.375 mg TBA) was added and boiled for another 15 min. After cooling, the flocculent precipitates were removed by centrifugation at 10,000*g* for 10 min. The absorbance of the supernatant was measured at 532 nm in a UV–Vis spectrophotometer to determine the level of lipid peroxidation. For GSH experiment, DTNB was used to determined intracellular GSH levels [34]. 1 mL of the bacterial suspension was collected by centrifugation and lysed by 100 μL of lysis buffer (KeyGEN BioTECH). 30 μL of cell extracts was mixed with 150 μL of 30 μg mL^{-1} DTNB for 25 min, and the absorbance at 412 nm that is proportional to the GSH level was measured using UV–Vis spectrophotometer.

Results and Discussion

Synthesis and ROS Generation of T, TG, TA, and TAG Under Sunlight Radiation

GO was synthesized by Hummers' method [29]. The TEM image, XRD pattern and IR spectrum (Figure S1) of GO clearly showed that GO had been successfully synthesized. Au NCs were synthesized according to a reported method [30]. The energy gap between HOMO and LUMO in Au NCs was 2.01 eV which was determined by UV–Vis diffuse reflectance spectra (Figure S2A-B) [35]. It implies that Au NCs could be excited by the photons with wavelength smaller than 617 nm, which was equal to 36.8% of sunlight energy according to the solar radiation spectrum. TEM image as well as the size-distribution histogram (Figure S2C-D) revealed that the primary size of Au NCs was 0.9 ± 0.1 nm. Au NCs were loaded on the surface of TiO_2 (T) NPs by electrostatic interaction between the positive charges of TiO_2 NPs and negative charges of carboxyl groups in Au NCs [36]. ICP-OES analysis showed the content of Au NCs in TA was 6.4%. TG and TAG were obtained through a hydrothermal method where T or TA

reacted with GO to form TG or TAG, respectively. Figure 2a showed the TEM images of T, TG, TA, and TAG. The diameter of TiO_2 NPs was about 20 nm with irregular shapes, and graphene or Au NCs could be clearly displayed on TG, TA and TAG nanocomposites. The size-distribution histogram (Figure S3) showed the size of Au NCs in TAG was similar with that of as-synthesized Au NCs, indicating that Au NCs can keep their original nature after formation of TAG nanocomposites. As shown in high resolution TEM (Fig. 2b) of TAG, typical wrinkle morphologies [37] of graphene could be displayed clearly, and the lattice fringes with interplanar distance of 0.35 and 0.24 nm were corresponding to the planes of TiO_2 (101) and Au NCs (111) [38]. In order to prove the electron transferring ability between Au NCs and TiO_2 NPs, the fluorescence emission of Au NCs (50 μg mL^{-1}) containing different concentrations of TiO_2 (0-1.6 mg mL^{-1}) was shown in Figure S4. The fluorescence intensity was decreased with increasing TiO_2 NP concentrations. When the concentration of TiO_2 reached to 1.6 mg mL^{-1}, the fluorescence of Au NCs was completely quenched. Figure 2c further shows the fluorescence emission of Au NCs, TA and TAG nanocomposites with equal contents of Au NCs, where the fluorescence intensity of TA was weaker than that of Au NCs and the fluorescence of TAG was completely quenched. It implied the exited electron of Au NCs can effectively transfer to TiO_2 NPs, and ultimately to graphene.

TAG was designed for improving ROS generation under sunlight radiation through sufficiently utilizing the solar energy and promoting the electron–hole separation. ROS generation on TAG compared to T, TG, and TA was examined by dihydrorhodamine 123 (DHR123) with or without sunlight radiation. Figure 2d shows that all the T, TG, TA and TAG nanomaterials could enhance the fluorescence intensity of DHR123 under sunlight radiation, and TAG exhibited the most potent fluorescence, followed by TA, TG and T, implying incorporation of Au NCs or graphene into TiO_2 NPs can significantly contribute to the

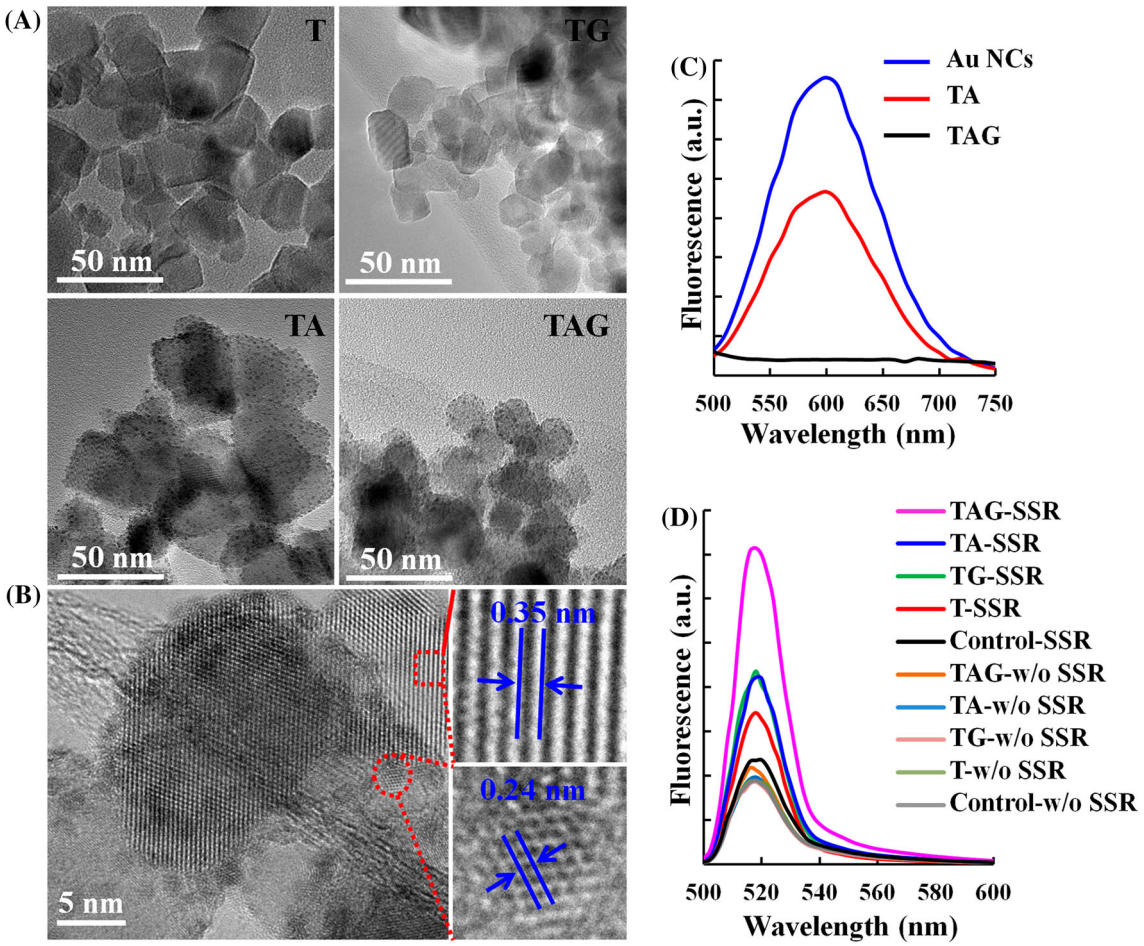

Fig. 2 Physicochemical properties of T, TG, TA, and TAG nanomaterials. **a** TEM images of T, TG, TA, and TAG nanomaterials; **b** High resolution TEM image of TAG; **c** Fluorescence emission spectra of Au NCs, TA and TAG (Ex = 420 nm) according to equal Au contents; **d** Fluorescence emission spectra of DHR123 (Ex = 490 nm) in the presence of T, TG, TA, and TAG (200 μg mL^{-1}, equal to TiO_2) with and without simulated sunlight radiation (SSR)

ROS generation of TiO_2 NPs. In comparison, without sunlight radiation, the fluorescence intensity of DHR123 was even weakened in the presence of T, TG, TA and TAG, meaning there is no ROS generation on these TiO_2-containing nanomaterials without sunlight radiation. In addition, ROS generation was also evaluated by another assay, DCF assay, and a similar trend was achieved (Figure S5), confirming the strongest ROS generation on TAG under sunlight radiation. All above results demonstrate TAG can efficiently generate ROS where Au NCs and graphene play crucial roles in free electron and hole formation.

Antibacterial Activity of T, TG, TA, and TAG

ROS can oxidize a range of biomolecules and damage cellular components such as lipids, protein and nucleic acids. The significantly enhanced ROS production on nanomaterials can lead to inactivation of bacteria. The antibacterial activity of T, TG, TA, and TAG according to their TiO_2 contents was examined in gram-negative *E. coli* and gram-positive *S. aureus* bacteria by investigating their growth kinetics. All these TiO_2-containing nanomaterials could be well dispersed in LB medium with hydrodynamic sizes at the range of 206.7 ± 28.9 to 348.5 ± 25.7 nm as determined by DLS (Table S1). Bacterial suspensions were incubated with a range of concentrations of T, TG, TA, and TAG for 30 min under sunlight radiation, and the subsequent bacterial growth was monitored by measurement of the optical density of bacterial suspension at 600 nm every hour. Bacterial viability assessments showed that all these TiO_2-containing nanomaterials exhibited remarkable dose-dependent inhibition against both *E. coli* and *S. aureus* bacterial growth (Fig. 3a), where TAG exhibited the strongest antibacterial activity, followed by TA, TG and T. This trend was consistent to their ROS generation trend. However, T, TG, TA and TAG did not exhibit antibacterial activity without sunlight radiation (Figure S6). In addition, Au NCs alone showed no antibacterial activity with or without sunlight radiation (Figure S7). The 0–6 h growth curves of *E. coli* and *S. aureus* in Fig. 3b (800 μg mL^{-1} of nanomaterials) and Figure S8 (400 μg mL^{-1} of nanomaterials) also clearly indicated the strongest inhibition ability of TAG among these TiO_2-containing nanomaterials under sunlight radiation, while Figure S9 revealed that non-antibacterial activity of these nanomaterials was shown without sunlight radiation. To corroborate the significant performance of TAG nanocomposites in inactivation of bacteria, the colony-forming capability of *E. coli* and *S. aureus* bacteria in LB agar plates was compared with or without sunlight radiation. As shown in Fig. 3c, TiO_2-containing nanomaterial-treated bacteria showed the significantly reduced the colony number, where TAG showed the most remarkable inhibition on the colony formation, and sunlight or Au NCs alone as a control treatment could not cause the photolysis of bacteria. Without sunlight radiation, all these nanomaterials could not reduce the colony number of bacteria (Figure S10). Meanwhile, the Live/Dead fluorescence staining assay of bacteria further revealed the strongest antibacterial activity of TAG with sunlight radiation (Fig. 3d) and their non-antibacterial activity without sunlight radiation (Figure S11). In addition, the morphological changes of *E. coli* and *S. aureus* bacteria were investigated using SEM technology. Figure 4 showed both untreated *E. coli* and *S. aureus* bacteria exhibited intact and smooth membranes. After 6 h of incubation with 200 μg mL^{-1} of TAG under sunlight radiation, the morphology of both types of bacteria was significantly changed. The bacterial membrane lost the integrity with a collapsed structure, leading to irreversible cell damage or cell death, revealing TAG can heavily damage the cell membranes of bacteria and cause cell death. All above results clearly demonstrate that TAG nanocomposites with the efficient ROS generation show the prominent antibacterial activity against both gram-negative and gram-positive bacteria under sunlight radiation. These results indicate the antibacterial activity of TiO_2 nanoparticles can be significantly enhanced by introducing of Au NCs, which can make full use of solar light with wavelength smaller 617 nm due to its narrow HOMO–LUMO energy gap. While in Au NPs-sensitized TiO_2 nanocomposites, solar light only with the wavelength near 550 nm can be absorbed due to the localized surface plasmon resonance (LSPR) effect of Au NPs. For example, it was reported that the free electrons and holes generating ability of Au/TiO_2 particles originated from activation of Au LSPR by light with wavelength at the range of 530–650 nm, which only utilized 15.6% of solar light [18, 39]. However, in Au NCs-sensitized TiO_2 nanocomposites introduced in the present study, about 36.8% of solar light can be utilized to generate free electrons and holes, which are a significant improvement compared with traditional Au NPs-sensitized TiO_2 nanocomposites. Besides, Au NCs can be uniformly engineered on TiO_2 NPs with high density with a simple method, which could favor the electron and hole transfer in the interface between Au NCs and TiO_2 NPs. As a result, the antibacterial activity can be increased with the help of Au NCs rather than Au NPs. In order to investigate the stability of TAG nanocomposies, TEM image of TAG was re-collected after sunlight irradiation (Figure S12), which shows the similar morphology with that before irradiation. Meanwhile, the mass ratio of Ti:Au:C determined by ICP-OES and elemental analyzer was 11.03:2.46:1 after irradiation, similar to that before irradiation (10.91:2.49:1). All above results demonstrate that the morphology and composition of TAG

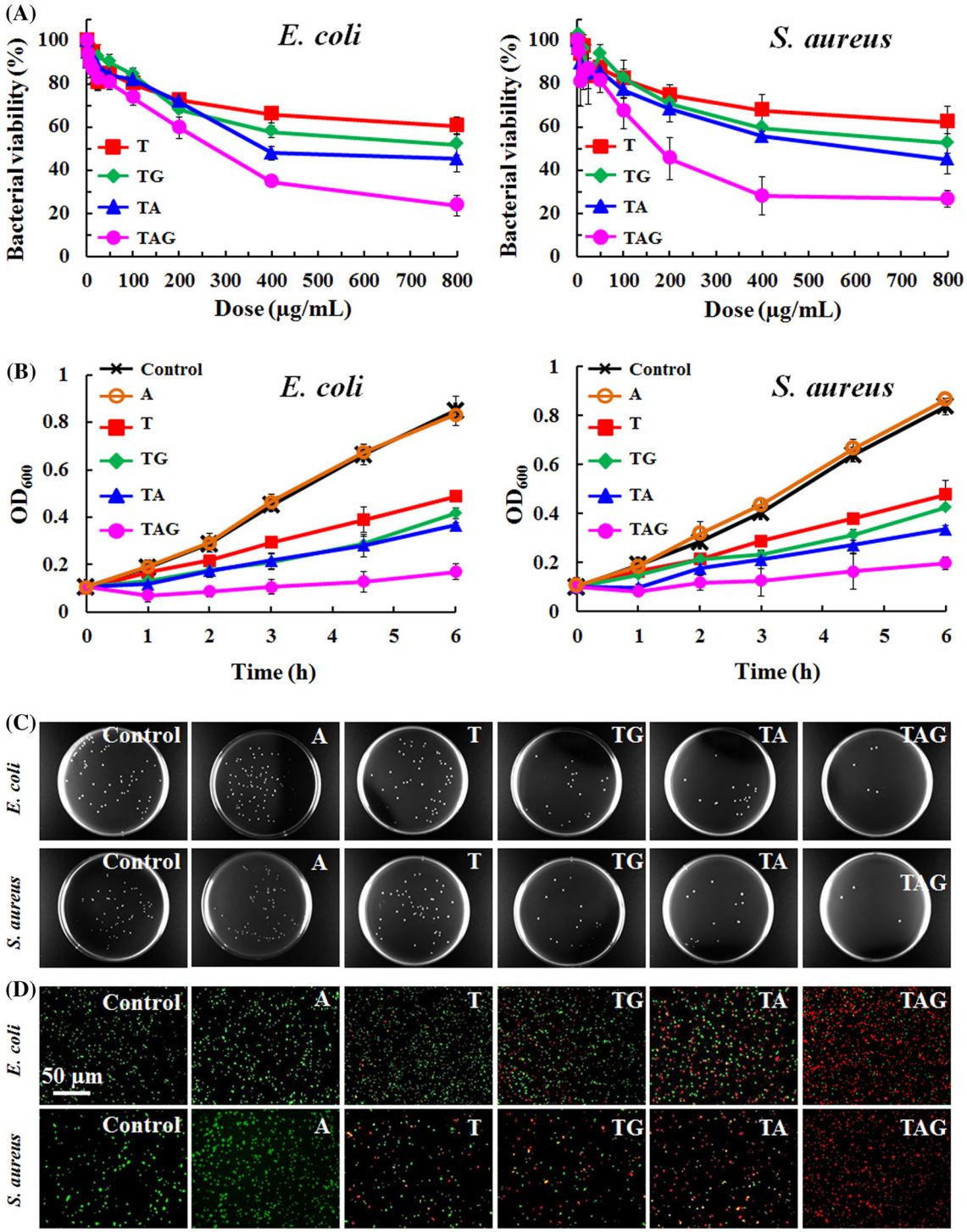

Fig. 3 Antibacterial activity of A, T, TG, TA, and TAG nanomaterials. **a** The bacterial viability of *E. coli* and *S. aureus* incubated with different doses of T, TG, TA, and TAG nanomaterials; **b** The 0–6 h growth curves of *E. coli* and *S. aureus* incubated with 51.2 μg mL^{-1} A or 800 μg mL^{-1} T, TG, TA, and TAG nanomaterials; The colony-forming capability **c** and Live (SYTO-9, green)/Dead (PI, red) staining **d** of *E. coli* and *S. aureus* incubated with 12.8 μg mL^{-1} A or 200 μg mL^{-1} T, TG, TA, and TAG nanomaterials. For **a**–**d**, the bacteria were radiated with simulated sunlight for 30 min and then incubated at 37 °C for 6 h (**a**, **b**, and **d**) or 24 h (**c**) on a rotary platform at a 160 rpm

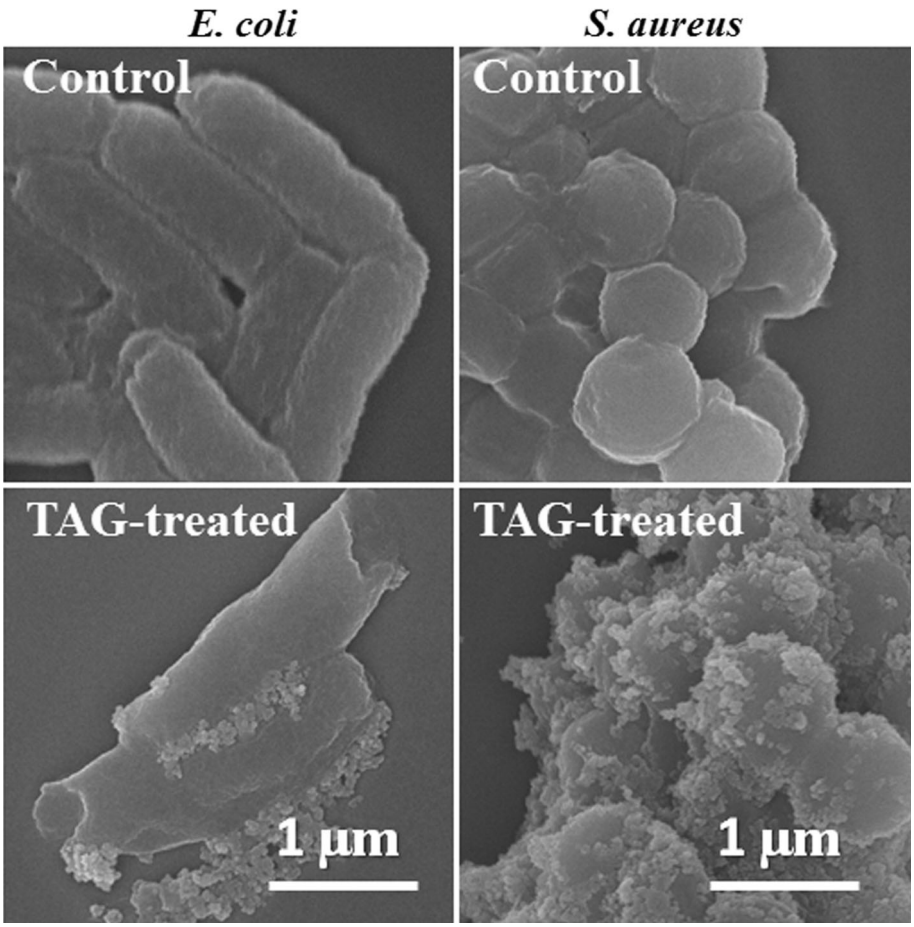

Fig. 4 SEM images of *E. coli* and *S. aureus* bacteria treated with 200 μg mL^{-1} TAG under simulated sunlight radiation for 30 min and incubated at 37 °C for 6 h on a rotary platform at a 160 rpm

cannot change after sunlight irradiation, indicating the excellent stability of TAG nanocomposites.

Molecular Mechanism Underlying the Antibacterial Activity of T, TG, TA, TAG

Since the antibacterial activity of T, TG, TA, and TAG showed a close correlation with their ROS generation, the oxidative stress was probably involved in the mechanism of bacterial inactivation. ROS generated on T, TG, TA and TAG can cause incremental ROS generation in bacteria through directly damaging the cell organelles and indirectly disturbing the equilibrium between oxidant and antioxidants process. Cellular ROS of bacteria was assessed by DCF, and the fluorescence images of *E. coli* and *S. aureus* bacteria were shown in Fig. 5a, b. TAG-treated bacteria exhibited the most potent fluorescence, followed with TA-, TG- and T-treated bacteria, implying incorporation of Au NCs or graphene into TiO_2 NPs can significantly contribute to the intracellular ROS generation. As is well known, ROS can damage the bacterial membrane through removing hydrogen atoms from the methylene groups on polyunsaturated fatty acid of bacterial membrane, leading to lipid peroxidation, ultimately to inactivation of bacteria [40]. The lipid peroxidation of bacteria can be assessed by their produced malondialdehyde (MDA) that can form an adduct with TBA and result in increased absorbance at 532 nm [41, 42]. Figure 5c showed all the T, TG, TA, and TAG could increase MDA levels in both *E. coli* and *S. aureus* bacteria under sunlight radiation and TAG exhibited the strongest lipid peroxidation effect. Without sunlight radiation, there was no MDA increase observed in the bacteria treated by any of these nanomaterials. In addition, significantly increased cellular ROS can ultimately overwhelm the antioxidant protection, leading to cellular GSH depletion. Intracellular GSH levels of *E. coli* and *S. aureus* bacteria treated with T, TG, TA and TAG were assessed by the DTNB assay [43]. Figure 5d indicated that T, TG, TA and TAG could obviously reduce GSH levels in both *E. coli* and *S. aureus* bacteria under sunlight radiation and TAG showed the strongest effect again. In addition, Au NCs alone could not induce cellular ROS generation, lipid peroxidation, and GSH depletion, proving their excellent biocompatibility. Based on ROS

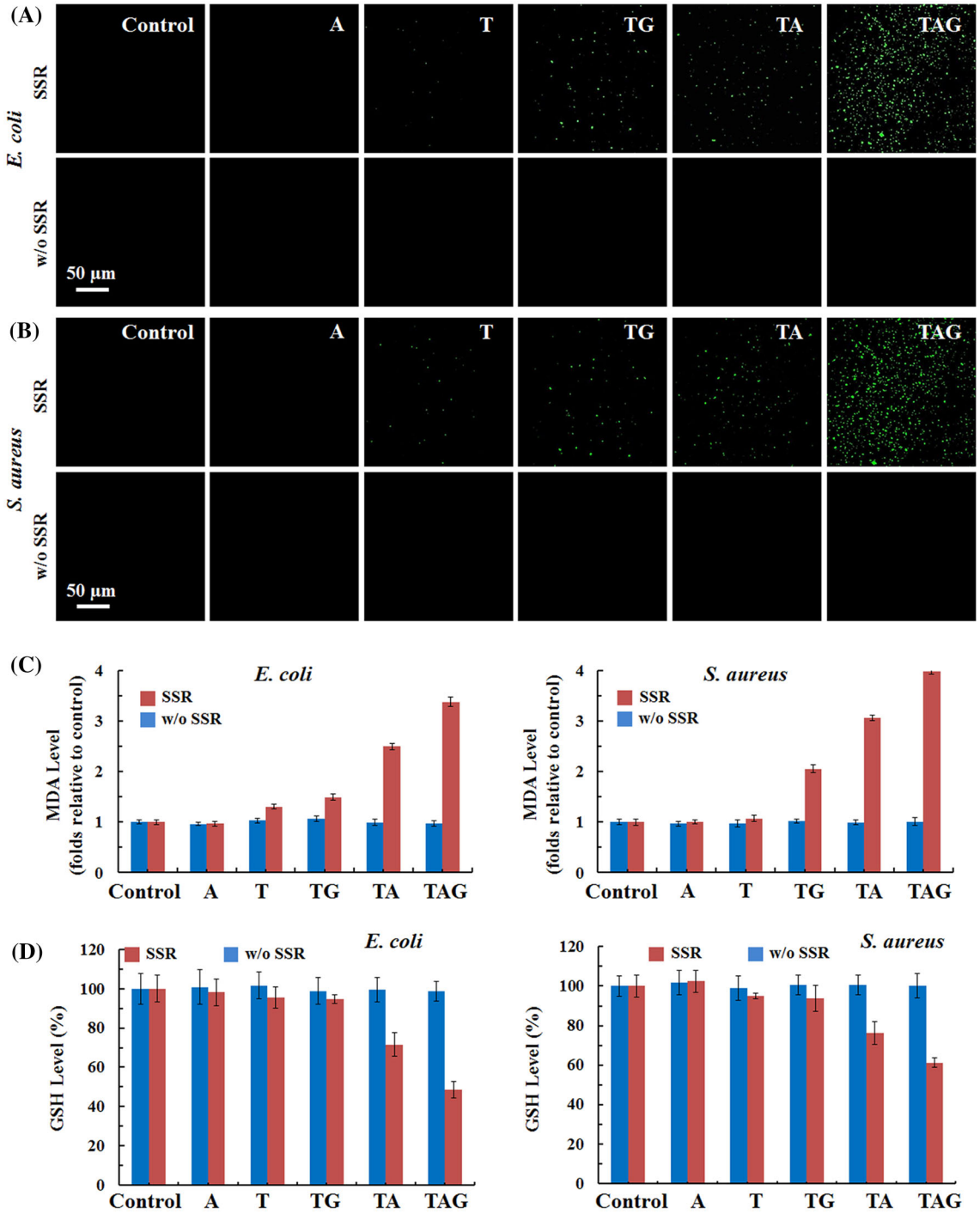

Fig. 5 Oxidative stress responses of *E. coli* and *S. auresus* bacteria treated with A, T, TG, TA, and TAG nanomaterials with or without SSR. Fluorescence images of *E. coli* (**a**) and *S. aureus* (**b**) bacteria stained by DCF; **c** Lipid peroxidation assessments of bacteria based on a MDA method; **d** GSH levels of bacteria determined by DTNB. Bacteria incubated with 12.8 μg mL^{-1} A or 200 μg mL^{-1} T, TG, TA, and TAG nanomaterials were radiated with or without simulated sunlight for 30 min, followed by 6 h incubation at 37 °C on a rotary platform at a 160 rpm

production, lipid peroxidation, and GSH depletion, the antibacterial activity of TAG is stimulated through oxidative stress signaling pathway.

Conclusion

In summary, Au NCs and graphene were incorporated into TiO_2 NPs to form unprecedented TAG nanocomposites used for enhancement of antibacterial activity of TiO_2 NPs. Incorporation of Au NCs and graphene could significantly enhance the solar energy utilization efficiency and promote the electron–hole separation of TiO_2 nanoparticles, leading to enhanced ROS production. Under sunlight radiation, TAG nanocomposites showed remarkable antibacterial activity against both *E. coli* and *S. aureus*, which were more potent than intrinsic TiO_2 NPs as well as TA and TG nanocomposites. The underlying mechanism of antibacterial activity of TAG nanocomposites was revealed through activation of oxidative stress.

Acknowledgements This work was primarily supported by the National Natural Science Foundation of China (21573216, 21703232, 21777152), Hundred Talent Program of CAS, Science and Technology Development Project Foundation of Jilin Province (20160101304JC, 20180520145JH).

References

1. M. J. Hajipour, K. M. Fromm, A. A. Ashkarran, D. Jimenez de Aberasturi, I. R. de Larramendi, T. Rojo, V. Serpooshan, W. J. Parak, and M. Mahmoudi (2012). *Trends Biotechnol.* **30**, 499.
2. Z. Lu, C. M. Li, H. Bao, Y. Qiao, Y. Toh, and X. Yang (2008). *Langmuir* **24**, 5445.
3. W. Hu, C. Peng, W. Luo, M. Lv, X. Li, D. Li, Q. Huang, and C. Fan (2010). *ACS Nano* **4**, 4317.
4. C. Marambio-Jones and E. M. V. Hoek (2010). *J. Nanopart. Res.* **12**, 1531.
5. K. H. Tam, A. B. Djurisic, C. M. N. Chan, Y. Y. Xi, C. W. Tse, Y. H. Leung, W. K. Chan, F. C. C. Leung, and D. W. T. Au (2008). *Thin Solid Films* **516**, 6167.
6. W. Bing, Z. W. Chen, H. J. Sun, P. Shi, N. Gao, J. S. Ren, and X. G. Qu (2015). *Nano Res.* **8**, 1648.
7. W. Wang, G. Li, D. Xia, T. An, H. Zhao, and P. K. Wong (2017). Environ. Sci. *Nano* **4**, 782.
8. J. C. Yu, W. Ho, J. Lin, H. Yip, and P. K. Wong (2003). *Environ. Sci. Technol.* **37**, 2296.
9. T. Paul, P. L. Miller, and T. J. Strathmann (2007). *Environ. Sci. Technol.* **41**, 4720.
10. R. A. Damodar, S. J. You, and H. H. Chou (2009). *J. Hazard. Mater.* **172**, 1321.
11. M. Radecka, M. Rekas, A. Trenczek-Zajac, and K. Zakrzewska (2008). *J. Power Sources* **181**, 46.
12. D. O. Scanlon, C. W. Dunnill, J. Buckeridge, S. A. Shevlin, A. J. Logsdail, S. M. Woodley, C. R. Catlow, M. J. Powell, R. G. Palgrave, I. P. Parkin, G. W. Watson, T. W. Keal, P. Sherwood, A. Walsh, and A. A. Sokol (2013). *Nat. Mater.* **12**, 798.
13. W. Curdt (2001). *AIP Conf. Proc.* **598**, 45.
14. J. C. Yu, W. Ho, J. Yu, H. Yip, P. K. Wong, and J. Zhao (2005). *Environ. Sci. Technol.* **39**, 1175.
15. O. Akhavan and E. Ghaderi (2010). *Surf. Coat. Technol.* **204**, 3676.
16. W. He, H. Huang, J. Yan, and J. Zhu (2013). *J. Appl. Phys.* **114**, 093710.
17. T. Nogawa, T. Isobe, S. Matsushita, and A. Nakajima (2012). *Mater. Lett.* **82**, 174.
18. E. Kowalska, O. O. P. Mahaney, R. Abe, and B. Ohtani (2010). *Phys. Chem. Chem. Phys.* **12**, 2344.
19. Y. Negishi, K. Nobusada, and T. Tsukuda (2005). *J. Am. Chem. Soc.* **127**, 5261.
20. Y. S. Chen and P. V. Kamat (2014). *J. Am. Chem. Soc.* **136**, 6075.
21. C. L. Yu, G. Li, S. Kumar, H. Kawasaki, and R. C. Jin (2013). *J. Phys. Chem. Lett.* **4**, 2847.
22. Y. Negishi, M. Mizuno, M. Hirayama, M. Omatoi, T. Takayama, A. Iwase, and A. Kudo (2013). *Nanoscale* **5**, 7188.
23. F. Fabregat-Santiago, I. Mora-Sero, G. Garcia-Belmonte, and J. Bisquert (2003). *J. Phys. Chem. B* **107**, 758.
24. I. Mora-Sero and J. Bisquert (2003). *Nano Lett.* **3**, 945.
25. K. S. Novoselov, A. K. Geim, S. V. Morozov, D. Jiang, M. I. Katsnelson, I. V. Grigorieva, S. V. Dubonos, and A. A. Firsov (2005). *Nature* **438**, 197.
26. K. S. Novoselov, A. K. Geim, S. V. Morozov, D. Jiang, Y. Zhang, S. V. Dubonos, I. V. Grigorieva, and A. A. Firsov (2004). *Science* **306**, 666.
27. J. S. Lee, K. H. You, and C. B. Park (2012). *Adv. Mater.* **24**, 1084.
28. J. C. Liu, L. Liu, H. W. Bai, Y. J. Wang, and D. D. Sun (2011). *Appl. Catal. B: Environ.* **106**, 76.
29. W. S. Hummers and R. E. Offeman (1958). *J. Am. Chem. Soc.* **80**, 1339.
30. Z. Luo, X. Yuan, Y. Yu, Q. Zhang, D. T. Leong, J. Y. Lee, and J. Xie (2012). *J. Am. Chem. Soc.* **134**, 16662.
31. M. Wrona, K. Patel, and P. Wardman (2005). *Free Radic. Biol. Med.* **38**, 262.
32. H. Zhang, S. Pokhrel, Z. Ji, H. Meng, X. Wang, S. Lin, C. H. Chang, L. Li, R. Li, B. Sun, M. Wang, Y. P. Liao, R. Liu, T. Xia, L. Madler, and A. E. Nel (2014). *J. Am. Chem. Soc.* **136**, 6406.
33. Y. Chang, K. Li, Y. Feng, N. Liu, Y. Cheng, X. Sun, Y. Feng, X. Li, Z. Wu, and H. Zhang (2016). *Nano Res.* **9**, 3812.
34. N. Liu, Y. Chang, Y. Feng, Y. Cheng, X. Sun, H. Jian, Y. Feng, X. Li, and H. Zhang (2017). *ACS Appl. Mater. Interfaces* **9**, 5907.
35. Y. Cheng, Y. Chang, Y. Feng, N. Liu, X. Sun, Y. Feng, X. Li, and H. Zhang (2017). *Small* **13**, 1603935.
36. N. Sakai and T. Tatsuma (2010). *Adv. Mater.* **22**, 3185.
37. Z. L. Wang, D. Xu, Y. Huang, Z. Wu, L. M. Wang, and X. B. Zhang (2012). *Chem. Commun. (Camb.)* **48**, 976.
38. C. Zhang, Z. Zhou, X. Zhi, Y. Ma, K. Wang, Y. Wang, Y. Zhang, H. Fu, W. Jin, F. Pan, and D. Cui (2015). *Theranostics* **5**, 134.
39. Y. Tian and T. Tatsuma (2005). *J. Am. Chem. Soc.* **127**, 7632.
40. Y. M. Zhang and C. O. Rock (2008). *Nat. Rev. Microbiol.* **6**, 222.
41. A. K. Chatterjee, R. Chakraborty, and T. Basu (2014). *Nanotechnology* **25**, 135101.
42. R. Chakraborty, R. K. Sarkar, A. K. Chatterjee, U. Manju, A. P. Chattopadhyay, and T. Basu (2015). *Biochim. Biophys. Acta* **1850**, 845.
43. T. Parandhaman, A. Das, B. Ramalingam, D. Samanta, T. P. Sastry, A. B. Mandal, and S. K. Das (2015). *J. Hazard. Mater.* **290**, 117.